9-2004

Volume Holographic Recording and Readout for 90-Deg Geometry

Partha P. Banerjee
University of Dayton, pbanerjee1@udayton.edu

Monish Ranjan Chatterjee
University of Dayton, mchatterjee1@udayton.edu

Nickolai Kukhtarev
Alabama A & M University

Tatiana Kukhtareva
Alabama A & M University

Volume holographic recording and readout for 90-deg geometry

Partha P. Banerjee, FELLOW SPIE
Monish R. Chatterjee, MEMBER SPIE
University of Dayton
Department of Electrical and Computer Engineering
Dayton, Ohio 45469
E-mail: partha.banerjee@notes.udayton.edu

Nickolai Kukhtarev, MEMBER SPIE
Tanya Kukhtareva
Alabama A&M University
Department of Physics
Normal, Alabama 36752

Abstract. When a prerecorded cross-beam hologram is reconstructed (so-called edge-lit readout) with a uniform plane wave and a point source, the resulting exact solutions reveal Bessel-function-type diffracted beam profiles, which are fundamentally modified under weak propagational diffraction. The case of a profiled beam readout with propagational diffraction may be analyzed using a transfer function approach based on 2-D Laplace transforms. In a second series of investigations, dynamic readout from a cross-beam volume hologram recorded with two orthogonal uniform plane waves is considered for various dependences of the refractive index modulation with intensity. Typically, refractive index profiles that are proportional to the intensity (as in the case of Kerr-type media or photorefractives with predominantly photovoltaic effect) and to the derivative of the intensity (as in diffusion-dominated photorefractives) are considered. Two-dimensional nonlinear coupled equations are developed for the two (Bragg) orders for both cases. Closed form solutions are obtained for the first case, indicating only nonlinearly induced self and cross-phase coupling. A simple experiment involving simultaneous recording and readout using photorefractive lithium niobate crystal indicates beam profile distortion, which may be expected in such 90-deg geometries. [DOI: 10.1117/1.1774195]

Subject terms: volume holographic recording; volume holographic readout; cross-beam hologram; 90-deg geometry; beam profile distortion; refractive index modulation.

Paper VHOE-B03 received Jan. 2, 2004; revised manuscript received Feb. 6, 2004; accepted for publication Feb. 6, 2004.

1 Introduction

Cross-beam or edge-lit holograms are of considerable current interest due to their potential compactness and inherent optical isolation between the readout beam and the diffracted order resulting from large Bragg angles.[1] Edge-lit holograms have been recorded in photorefractive materials, including lithium niobate crystals, using novel multiplexing techniques.[2–4] Numerous applications of the edge-lit technique are possible, including holographic optical elements such as diffusers, reflectors, and backscattering plates in display systems, 3-D object displays, and display screens for holographic projectors and video.[5,6] To achieve flexibility in display devices, edge-lit holograms must be multiplexed for efficient modulation. Owing to the special configurations involved here, which do not conform to conventional holographic multiplexing techniques, novel multiplexing techniques suitable for edge-lit holography have recently been developed.[7]

In Sec. 2, we consider reconstruction from edge-lit holograms prerecorded with uniform plane waves. Using paraxial optics and the slowly varying envelope approximation (SVEA), first-order coupled equations are derived for the diffracted orders in the two mutually orthogonal directions, in the absence of propagational diffraction. Given the orthogonal propagation of the two orders, the resulting coupled equations may be converted into 2-D Laplace transformed equations representing the complex spectra of the scattered orders. For the two special cases of uniform plane wave readout (here assumed to correspond to a unit step profile along one of the input planes), and a point source (or delta-function) readout, the resulting diffracted beam profiles are found to be different versions of zeroth and first-order Bessel functions of the first kind. It is rather serendipitous that in these two instances, the derived 2-D Laplace spectra are invertible via straightforward series expansion methods. When the coupled equations are modified to include propagational diffraction in each of the orthogonal directions, the resulting 2-D angular plane wave spectra are found to be expressible as the product of the spectrum of the incident zeroth-order reading profile, and zeroth- and first-order 2-D transfer functions (in the manner of linear systems), respectively. These transfer functions technically enable one to find the diffracted beam profiles for arbitrary reading beam profiles. A primary difficulty in attempting to solve the spatial diffracted profiles for these 2-D spectral representations is the complexity of performing inverse Laplace transforms of dimensions greater than 1. A simple illustration of the effect of propagational diffraction is provided by considering weak diffraction, where by using appropriate simplifications, the intermediate inverse transform over one of the orthogonal directions yields a 1-D Laplace result that deviates from the corresponding one in the absence of propagational diffraction via polynomial phase

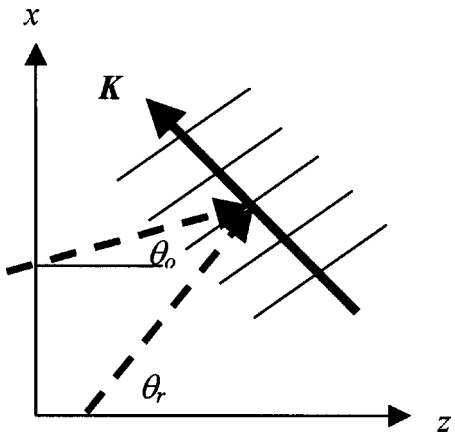

Fig. 1 General edge hologram recording geometry.

terms in the surviving Laplace variable. It is pointed outthat the inverse transformation of 2-D Laplace functions as derived here is rather difficult even under weak diffraction limits, even for uniform plane wave or point source reading beams (and considerably more so for arbitrary reading beam profiles). Attempting conventional numerical integration (simultaneously, or one dimension at a time) leads invariably to problems involving singularities of the transfer functions and (likely) of the incident plane wave spectrum. It turns out, however, that some researchers have recently attempted to find inverse Laplace transforms of multidimensional Laplace functions.[8,9] The essence of one such technique is briefly discussed. In a follow-up work, results obtained by using such an inversion technique will be presented.

In Sec. 3, governing equations are derived for the self-readout of a dynamic hologram under 1. intensity-dependent refractive index modulation (as is true for a Kerr-type material or a photorefractive material with strong photovoltaic effect); and 2. intensity gradient-dependent refractive index modulation (as in a diffusion-dominated photorefractive medium) of the volume holographic material. For the first case, solution of the Helmholtz equation under SVEA and weak propagational diffraction indicates that the intensities of the scalar zeroth- and first-order beams depend only on their respective initial intensities at the input planes. Their phases, however, evolve as combinations of both self-phase (i.e., due to the incident intensity of the field itself) and cross-phase (due to the incident intensity of the orthogonal field) modulations. For the second case, application of the index modulation to the Helmholtz equation, on simplification, reduces to two nonlinearly coupled first-order intensity and phase equations. The solutions, subject to initial zeroth- and first-order intensity conditions, are quite involved, and will be pursued later.

Preliminary experimental results for dynamic recording and readout of edge-lit holograms in photorefractive lithium niobate indicate profile distortion under Gaussian beam input conditions. The results, shown in Sec. 4, suggest that the contribution from diffusion in the holographic recording and readout process in the material may not be negligible.

2 Reconstruction of Prerecorded Thick Holograms for Cross-Beam Geometry

Consider a hologram, as shown in Fig. 1, which is recorded by interference of two uniform plane waves as[10]

$$\varepsilon(x,z)=\varepsilon_1+\varepsilon_2\cos(\vec{K}\cdot\vec{r}), \tag{1}$$

where the grating vector is

$$\vec{K}=K\cos\phi\vec{a}_z+K\sin\phi\vec{a}_x, \tag{2}$$

and

$$K=2k\sin\frac{\theta_r-\theta_o}{2}, \tag{3}$$

where k refers to a propagation constant of light in the material, to be made more precise later. Also, the angle of the grating vector is

$$\phi=\pi/2+(\theta_r+\theta_o)/2, \tag{4}$$

where θ_r and θ_o are the incident angles of the reference and object waves, respectively.

During reconstruction, the total optical field phasor in the volume hologram (assumed to have two orders) can be expressed as:

$$\begin{aligned}\psi(x,z)&=[\psi_{e0}(x,z)\exp-j\vec{k}_0\cdot\vec{r}+\psi_{e1}(x,z)\exp-j\vec{k}_1\cdot\vec{r}]\\&=[\psi_{e0}(x,z)\exp-j(k_{0x}x+k_{0z}z)\\&\quad+\psi_{e1}(x,z)\exp-j(k_{1x}x+k_{1z}z)],\end{aligned} \tag{5}$$

with

$$k_{0x}=k\sin\theta_r,\quad k_{0z}=k\cos\theta_r,\quad k_{1x}=k\sin\theta_r-K\sin\phi,$$

$$k_{1z}=k\cos\theta_r-K\cos\phi, \tag{6}$$

where $k=2\pi\sqrt{\varepsilon_1}/\lambda_2$ is the propagation constant of the reconstruction wave.

Substituting Eqs. (5) and (6) into the Helmholtz equation along with Eqs. (1) through (4), we get:

$$\nabla^2\psi_{e0}-2j\vec{k}_0\cdot\vec{\nabla}\psi_{e0}+\frac{k^2\varepsilon_2}{2\varepsilon_1}\psi_{e1}=0, \tag{7}$$

$$\nabla^2\psi_{e1}-2j\vec{k}_1\cdot\vec{\nabla}\psi_{e1}+\frac{k^2\varepsilon_2}{2\varepsilon_1}\psi_{e0}-2k\Theta\psi_{e1}=0, \tag{8}$$

where Θ is a dephasing factor, dependent on the angle of the reading beam ψ_{e0}. Equations (7) and (8) represent the coupled wave equations for the two diffracted orders.

Suppose we now assume the following recording parameters: 1. the hologram is recorded with $\theta_r=\pi/2$, $\theta_o=0$, which implies $K=\sqrt{2}k$ and $\phi=3\pi/4$; and 2. the hologram is confined between boundary planes specified by $z=0$, $z=L$; $x=0$, $x=L$; where we have assumed a square of size L. Likewise, we assume the reading parameters to be those for nominal Bragg incidence, so that $k_{0x}=k$, $k_{0z}=0$, k_{1x}

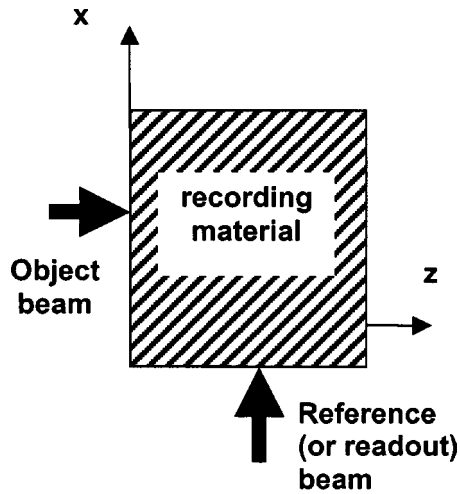

Fig. 2 Typical 90-deg recording geometry leading to gratings at 45 deg. Subsequent readout using a beam in the direction of the reference beam.

$=0$, $k_{1z}=k$; $\Theta=0$. Substituting the parameters in Eqs. (7) and (8), and assuming only plane wave interaction (no propagational diffraction) and SVEA, we obtain the following reduced coupled equations:

$$\partial\psi_{e0}/\partial x=-j\kappa\psi_{e1},$$

$$\partial\psi_{e1}/\partial z=-j\kappa\psi_{e0}, \tag{9}$$

where $\kappa=k\varepsilon_2/4\varepsilon_1$. The schematic diagram showing the volume hologram and the reconstruction is shown in Fig. 2.

Note that the previous coupled equations are similar to the standard ideal Bragg scattering equations in acousto-optic diffraction, except that the derivatives on the left hand side (LHS) are in two (orthogonal) directions instead of one. Hence, the solutions are also expected to be significantly different, as is shown later.

2.1 *Case 1: Uniform Plane Wave Readout*

Consider the initial conditions for the zeroth and first orders at $x=0$ and $z=0$, respectively:

$$\psi_{e0}(0,z)=Cu(z),\psi_{e1}(x,0)=0,$$

where $u(z)$ is a unit step in the z direction, and C is a constant.

To solve Eq. (9), we Laplace transform the coupled equations in 2-D between (x,z) and (s_x,s_z) to obtain:

$$s_x\Psi_{e0}(s_x,s_z)-\tilde{\Psi}_{e0}(x=0,s_z)=-j\kappa\Psi_{e1}(s_x,s_z),$$

$$s_z\Psi_{e1}(s_x,s_z)-\tilde{\Psi}_{e1}(s_x,z=0)=-j\kappa\Psi_{e0}(s_x,s_z), \tag{10}$$

where the second terms on the LHS of Eq. (10) are the 1-D Laplace transforms of the reading initial conditions at the input planes. Using the initial conditions from before, we finally obtain:

$$\Psi_{e0}(s_x,s_z)=\frac{C}{s_xs_z+\kappa^2},$$

$$\Psi_{e1}(s_x,s_z)=-\frac{j\kappa C}{s_z(s_xs_z+\kappa^2)}. \tag{11}$$

The solutions in the spatial domain are found by inverse Laplace transforming the prior expressions. For instance, inverse Laplace transforming the first of the equations in Eq. (11) with respect to s_x, we get

$$\tilde{\Psi}_{e0}(x,s_z)=\frac{C}{s_z}\exp(-\kappa^2x/s_z),$$

which can be inverse transformed with respect to s_z (using a power series expansion) to give:

$$\psi_{e0}(x,z)=CJ_0(2\kappa\sqrt{xz}). \tag{12}$$

In a similar manner, the second of the expressions in Eq. (11) can be inverse Laplace transformed to give, after some algebra:

$$\psi_{e1}(x,z)=jC\sqrt{\frac{z}{x}}J_1(2\kappa\sqrt{xz}). \tag{13}$$

Typical solutions (normalized to the incident reading wave amplitude) are plotted in Fig. 3 at the respective output planes of the hologram.

2.2 *Case 2: Delta Function or Point Source Readout*

For initial conditions

$$\psi_{e0}(0,z)=C\delta(z-z_0),\psi_{e1}(x,0)=0,$$

Eq. (10) yields

$$\Psi_{e1}(s_x,s_z)=-\frac{j\kappa C}{(s_xs_z+\kappa^2)}\exp(-z_0s_z). \tag{14}$$

Inverse Laplace transforming with respect to s_x gives

$$\hat{\Psi}_{e1}(x,s_z)=-\frac{j\kappa C}{s_z}\exp(-\kappa^2x/s_z)\exp(-z_0s_z).$$

It is interesting to note that the inverse Laplace transform with respect to s_z will now give a result similar to Eq. (12) (which is the result for the undiffracted order for uniform plane wave readout), except with shifted coordinates:

$$\psi_{e1}(x,z)=-j\kappa CJ_0\{2\kappa[x(z-z_0)]^{1/2}\}. \tag{15}$$

2.3 *Case 3: Readout in the Presence of Propagational Diffraction*

Strictly speaking, the analysis in case 2 for a point source should have included the effect(s) of propagational diffraction. Using the same reading parameters as before, but now including propagational diffraction and SVEA, the coupled PDEs become:

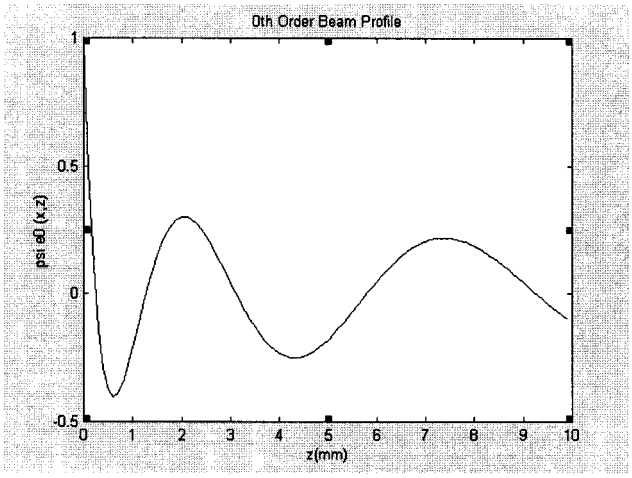

(a)

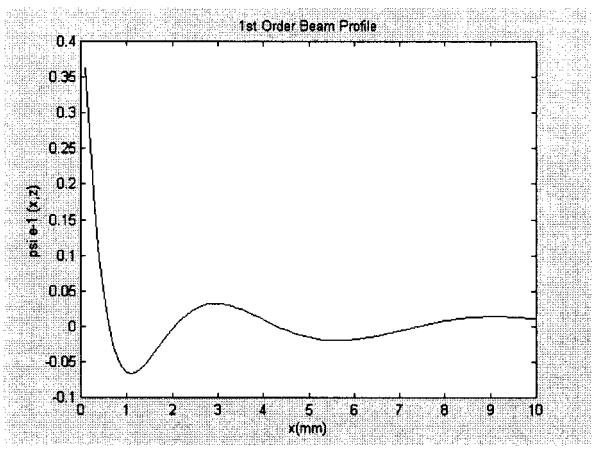

(b)

Fig. 3 Typical plots for (a) zero- and (b) first-order diffraction profiles with uniform plane wave readout; wavelength=633 nm, refractive index=1.6, $\varepsilon_2=0.0005$, and crystal dimension $L=1$ cm.

$$\partial\psi_{e0}/\partial x=-j\kappa\psi_{e1}+\frac{1}{2jk}\partial^2\psi_{e0}/\partial z^2,$$

$$\partial\psi_{e1}/\partial z=-j\kappa\psi_{e0}+\frac{1}{2jk}\partial^2\psi_{e1}/\partial x^2. \tag{16}$$

These represent wave coupling under the paraxial approximation.

Let us assume initial and/or boundary conditions as

$$\psi_{e0}(0,z)=f_0(z),\psi_{e1}(x,0)=0;$$

$$\psi_{e0}(x,0)=0,\psi_{e1}(0,z)=0;$$

$$\left.\frac{\partial\psi_{e0}(x,z)}{\partial z}\right|_{z=0}=0,\quad \left.\frac{\partial\psi_{e1}(x,z)}{\partial x}\right|_{x=0}=0. \tag{17}$$

Laplace transforming Eq. (16) with respect to x and z, using Eq. (17), and after extensive algebra, we get

$$\Psi_{e0}(s_x,s_z)=\frac{s_z-\frac{s_x^2}{2jk}}{\left(s_x-\frac{s_z^2}{2jk}\right)\left(s_z-\frac{s_x^2}{2jk}\right)+\kappa^2}F_0(s_z)$$
$$=H_0(s_x,s_z)F_0(s_z),$$

$$\Psi_{e1}(s_x,s_z)=\frac{-j\kappa}{\left(s_x-\frac{s_z^2}{2jk}\right)\left(s_z-\frac{s_x^2}{2jk}\right)+\kappa^2}F_0(s_z)$$
$$=H_1(s_x,s_z)F_0(s_z), \tag{18}$$

where $F_0(s_z)$ is the Laplace transform of $f_0(z)$ with respect to z. The previous relations can be reworked for arbitrary initial conditions in Eq. (17).

For weak propagational diffraction, the second of the relations in Eq. (18) reduces to:

$$\Psi_{e1}(s_x,s_z)\approx\frac{-j\kappa}{\left(s_xs_z-\frac{s_z^3}{2jk}-\frac{s_x^3}{2jk}\right)+\kappa^2}F_0(s_z). \tag{19}$$

Furthermore, on replacing s_x in the cubic term with $-\kappa^2/s_z$ (assuming weak propagational diffraction once again, so that in the first approximation the pole in the s_x plane is at $-\kappa^2/s_z$) and taking the inverse Laplace transform with respect to s_x, we get, for the case of a point source readout:

$$\hat{\Psi}_{e1}(x,s_z)=-\frac{j\kappa C}{s_z}\exp(-\kappa^2x/s_z)[\exp(j\kappa^6x/2ks_z^4)$$
$$\times\exp(-js_z^2x/2k)]\exp(-z_0s_z). \tag{20}$$

Comparing with the solution in Eq. (14), which was found neglecting diffraction, namely,

$$\hat{\Psi}_{e1}(x,s_z)=-\frac{j\kappa C}{s_z}\exp(-\kappa^2x/s_z)\exp(-z_0s_z),$$

we find additional terms [indicated by the term in square brackets in Eq. (20)] due to the presence of propagational diffraction.

Exact analytical solutions of Eqs. (19) or (20) cannot be found; one has to resort to numerical methods to find the inverse Laplace transform. Numerical methods for inverse Laplace transforms have been a topic of recent interest for investigating problems in stochastic modeling and operations research.[8,9] The solutions can be symbolically written as:

$$\psi_e(x,z)=\frac{\exp(c_xx+c_zz)}{4\pi^2}\int_{-\infty}^{\infty}\int_{-\infty}^{\infty}[\Re\Psi_e(c_x+jk_x,c_z+jk_z)$$
$$\times\cos(k_xx+k_zz)-\Im\Psi_e(c_x+jk_x,c_z+jk_z)$$
$$\times\sin(k_xx+k_zz)]\mathrm{d}k_x\mathrm{d}k_z, \tag{21}$$

where $\Re$ denotes the "real part of," and $\Im$ denotes the "imaginary part of." In Eq. (21), one needs to choose $c_x > d_x$, $c_z > d_z$, where $\Psi_e(s_x, s_z)$ is analytic for $\Re s_x > d_x$, $\Re s_z > d_z$. We plan to pursue this in the future.

3 Analysis of Dynamic Recording and Readout for 90-Deg Geometry

In this case, the hologram is assumed to be simultaneously recorded and read out in a two-wave mixing geometry, with the interacting waves traveling nominally at 90 deg to each other. The starting point is the Helmholtz equation for the phasor optical field $\psi(x,z)$:

$$\frac{\partial^2\psi}{\partial x^2}+\frac{\partial^2\psi}{\partial z^2}+k^2n^2(x,z)\psi=0, \tag{22}$$

where $n=n_0+\Delta n$ is the overall refractive index, with Δn representing the induced refractive index, and k now denotes the propagation constant in vacuum. Assuming small modulation, Eq. (22) can be restated as

$$\frac{\partial^2\psi}{\partial x^2}+\frac{\partial^2\psi}{\partial z^2}+k^2n_0^2(x,z)\psi+2n_0k^2\Delta n\psi=0. \tag{23}$$

It can be shown that the change in refractive index can be expressed as

$$\Delta n=n_2|\psi|^2, \tag{24}$$

for the case of a Kerr-type material or a photorefractive material such as $LiNbO_3$, where the photovoltaic effect dominates, and we have assumed that the intensity interference pattern is smaller than the dark current and/or the background intensity.[10] On the other hand, in the case where diffusion is the dominant mechanism for charge transfer in a photorefractive material, the change in the refractive index is proportional to the gradient of the intensity[11] and can be expressed as:

$$\Delta n=n_{21}\frac{\partial|\psi|^2/\partial x}{C+|\psi|^2}+n_{23}\frac{\partial|\psi|^2/\partial z}{C+|\psi|^2}, \tag{25}$$

where C is a constant that depends on the dark current and any background illumination on the material. Note also that the right hand side (RHS) of Eq. (25) represents an estimate of the electrostatic field, which is related to the induced refractive index through the index ellipsoid. In our analysis, we have assumed that Δn is an effective change in the refractive index, which depends on the x and z derivatives of the overall intensity. In the case where the contribution of the intensity interference pattern is smaller than that of the dark current and/or the background intensity, i.e., $C \gg |\psi|^2$, Eq. (25) can be simplified to yield:

$$\Delta n=n_{21}\partial|\psi|^2/\partial x+n_{23}\partial|\psi|^2/\partial z, \tag{26}$$

where we have absorbed an additional constant in the n_2s.

3.1 *Case 1: Wave Coupling in Kerr or Photovoltaic Materials*

Assume the total scalar optical field is expressible in the form

$$\psi=\frac{1}{2}\psi_{e0}(x,z)\exp-jn_0kx+\frac{1}{2}\psi_{e1}(x,z)\exp-jn_0kz. \tag{27}$$

After extensive algebra on using Eq. (24) in Eq. (23), and equating the coefficients of $\exp-jn_0kx$, $\exp-jn_0kz$ separately to zero, we get, respectively,

$$\frac{\partial^2\psi_{e0}}{\partial x^2}+\frac{\partial^2\psi_{e0}}{\partial z^2}-2jn_0k\frac{\partial\psi_{e0}}{\partial x}+\frac{1}{2}n_0n_2k^2[|\psi_{e0}|^2+2|\psi_{e1}|^2]\psi_{e0}=0, \tag{28}$$

$$\frac{\partial^2\psi_{e1}}{\partial x^2}+\frac{\partial^2\psi_{e1}}{\partial z^2}-2jn_0k\frac{\partial\psi_{e1}}{\partial z}+\frac{1}{2}n_0n_2k^2[|\psi_{e1}|^2+2|\psi_{e0}|^2]\psi_{e1}=0. \tag{29}$$

Now, similar to the SVEA used in propagation problems, we can neglect the second derivative with respect to x as compared to the term involving the first derivative in x in Eq. (28). Strictly speaking, the second term on the LHS of Eq. (28) represents the propagational diffraction of the beam as it propagates along x; however, we assume that the initial beam size is large enough so that the Rayleigh range of the beam is much larger than the interaction length in the crystal; hence, this diffraction term may be neglected. With these assumptions, Eq. (28) reduces to:

$$\frac{\partial\psi_{e0}}{\partial x}=-j\frac{1}{4}n_2k[|\psi_{e0}|^2+2|\psi_{e1}|^2]\psi_{e0}. \tag{30}$$

Similarly, Eq. (29) reduces to:

$$\frac{\partial\psi_{e1}}{\partial z}=-j\frac{1}{4}n_2k[|\psi_{e1}|^2+2|\psi_{e0}|^2]\psi_{e1}. \tag{31}$$

Equations (30) and (31) can be solved for the amplitude and phase of the interacting waves in the following way. Note that by multiplying Eq. (30) by ψ_{e0}^* we get:

$$\psi_{e0}^*\frac{\partial\psi_{e0}}{\partial x}=-j\frac{1}{4}n_2k[|\psi_{e0}|^2+2|\psi_{e1}|^2]|\psi_{e0}|^2.$$

Now, taking the complex conjugate of this equation and adding the two equations, we get

$$\frac{\partial|\psi_{e0}|^2}{\partial x}=0,$$

which implies:

$$|\psi_{e0}|^2=f_0^2(z), \tag{32}$$

where $f_0^2(z)$ is an integration constant and equal to the initial intensity profile of the field ψ_{e0}. In a similar manner it can be shown that

$$|\psi_{e1}|^2=f_1^2(x), \tag{33}$$

where $f_1^2(x)$ is the initial intensity profile of the field ψ_{e1}. To solve for the phases, we assume

$$\psi_{e0}(x,z)=f_0(z)\exp-j\phi_0(x,z),$$

$$\psi_{e1}(x,z)=f_1(x)\exp-j\phi_1(x,z), \tag{34}$$

and substitute in Eqs. (30) and (31) to obtain the pair of differential equations

$$\frac{\partial\phi_0}{\partial x}=\frac{1}{4}k_0n_2[f_0^2(z)+2\,f_1^2(x)], \tag{35}$$

$$\frac{\partial\phi_1}{\partial z}=\frac{1}{4}k_0n_2[2\,f_0^2(z)+f_1^2(z)]. \tag{36}$$

Equation (35) suggests that the accumulated phase for ψ_{e0} during travel by a distance x through the interaction region has a part due to self-phase modulation, which is dependent on the transverse dimension z, and a part due to cross-phase modulation, which is dependent on the longitudinal dimension x. Similar arguments can be made for the accumulated phase of ψ_{e1}. Accordingly, any change in the profile of the far-field intensity distribution of ψ_{e0} (which is proportional to the spatial Fourier transform with respect to z of the exit profile at the end of the interaction region) is expected to be only due to the initial beam profile of ψ_{e0} itself, and is not affected by the initial beam profile of ψ_{e1}, since the latter is a function of x. A similar argument can be advanced for the far-field intensity distribution of ψ_{e1} after passage through the interaction region.

3.2 *Case 2: Wave Coupling in Diffusion-Dominated Materials*

In this case, the coupled equations can be shown to be of the form

$$\frac{\partial\psi_{e0}}{\partial x}=-\gamma|\psi_{e1}|^2\psi_{e0}, \tag{37}$$

$$\frac{\partial\psi_{e1}}{\partial z}=\gamma|\psi_{e0}|^2\psi_{e1}, \tag{38}$$

where γ is a beam coupling coefficient, related to the n_2s in Eq. (26). We can assume ψ_{e0},ψ_{e1} to be real, and rewrite the previous set of coupled equations in terms of the intensities I_0,I_1 in the form

$$\frac{\partial I_0}{\partial x}=-\gamma I_0I_1=-\frac{\partial I_1}{\partial z}. \tag{39}$$

The solution of this set of equations, subject to the initial conditions $I_0\ (x=0,z)$, $I_1\ (x,z=0)$ is involved, and will be pursued in the future.

4 Preliminary Experimental Results

We have made experiments with edge-lit holographic recording in a 1-cm^3 crystal of Fe-doped $LiNbO_3$, using a He-Ne laser (wavelength 632 nm). Two unexpanded near-Gaussian beams from a low-power (15 mW) He-Ne laser are made to intersect in the crystal at 90 deg, as shown in Fig. 4. All laser beams are polarized out of the plane of the paper, to avoid large nonlinear holographic scattering. The C axis of the crystal is in the plane of the paper and along the direction of propagation of one of the beams (see Fig. 4). Transverse intensity profiles of the two intersecting beams are measured by a beam profiler. The goal of this experiment is to check qualitatively the theoretical predictions about spatial redistributions of beam intensity after diffraction by holographic gratings, recorded in a 90-deg geometry.

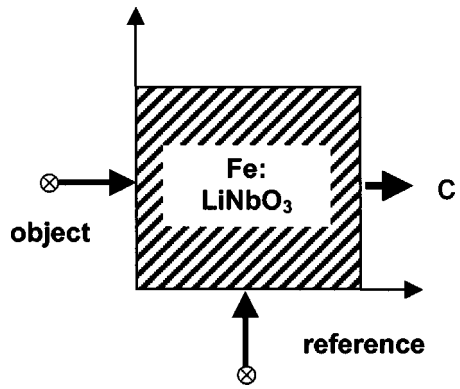

Fig. 4 Schematic experimental setup using Fe:$LiNbO_3$ for simultaneous recording and reconstruction of a hologram at 90-deg geometry. Polarization of both beams are perpendicular to the paper and the C axis.

Figure 5(a) shows the intensity profile for one of the input beams. This distribution is close to a Gaussian distribution, as expected. In Fig. 5(b) we demonstrate the intensity profile of one of the transmitted beams (traveling along the C axis) after grating recording. Figure 5(c) shows intensity of the other beam profile (that is normal to the C axis), after grating recording. We can see substantial spatial modulation, induced by the recorded holographic grating. This leads us to believe that contribution from diffusion leading to energy exchange in $LiNbO_3$ may not be negligible, since the photovoltaic contribution by itself (as modeled) should not cause beam profile distortion, as predicted from our previous theoretical model. Furthermore, large modulation effects can also affect the dependence of the refractive index on the intensity profile, as predicted by Kukhtarev et al.[11] The observed random distortions in the experimental results (see Fig. 5) can be better analyzed only if we introduce noise terms into the interaction equations. At this preliminary stage of investigation, these terms were omitted, and they will be considered in the future.

5 Discussions

We investigate some aspects of holographic recording and reconstruction for edge-lit holograms. Beam shaping in the case of plane wave readout from a previously recorded planar hologram is predicted. It is also shown that in a simultaneous recording-readout configuration, Kerr-type materials (or photorefractive materials with predominantly photovoltaic effect) should not alter the transverse shape of the beam profiles. However, there is a strong possibility that beam shape distortion will occur in a diffusion-dominated photorefractive material. This is also observed in our experimental results of volume holographic recording and reconstruction using a Fe-doped $LiNbO_3$ crystal,

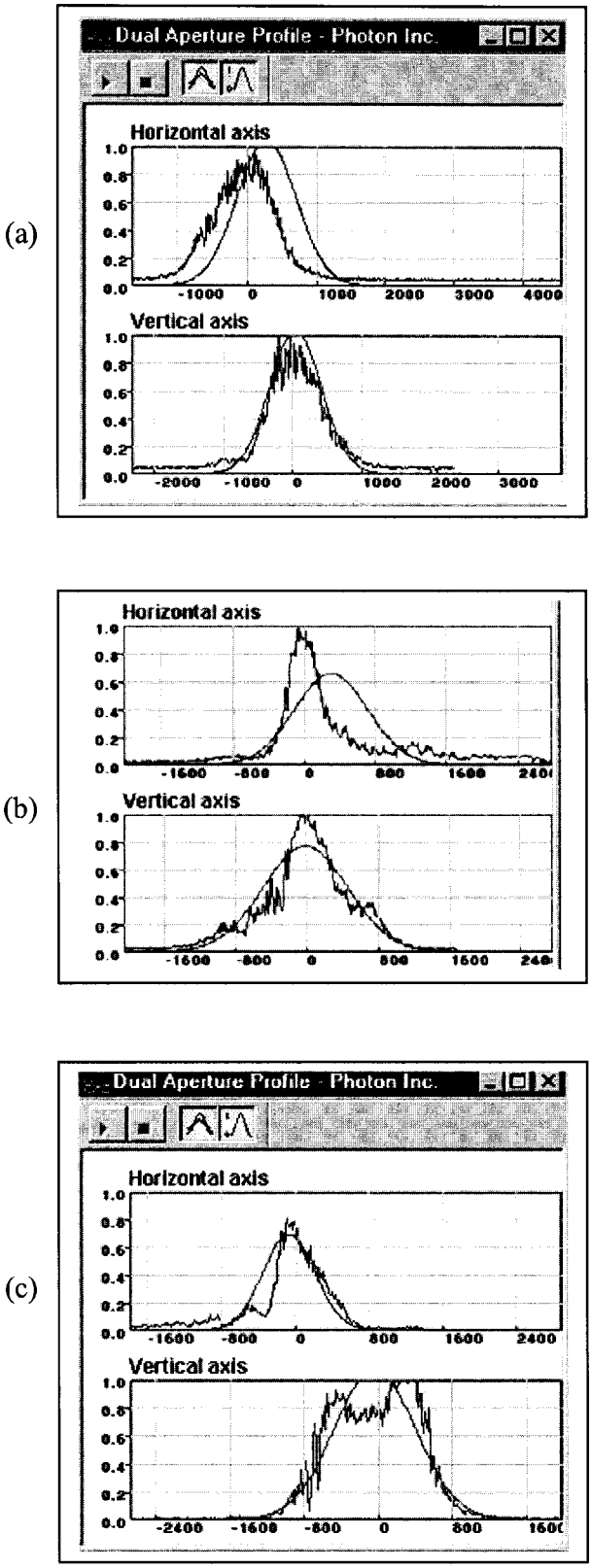

Fig. 5 Dynamic holographic recording and reconstruction in photorefractive lithium niobate using cross-beam geometry: (a) typical intensity profile for the input beams; (b) intensity profile of the beam traveling along the *C* axis after grating recording; and (c) intensity profile of the beam traveling normal to the *C* axis after grating recording. All beam profiles were monitored using a Spiricon beam profiler.

suggesting that diffusion effects may not be negligible. Cases of recording and readout that incorporate propagational diffraction have been modeled, and will be solved using a 2-D Laplace transform approach in the near future.

References

1. H. Ueda, E. Shimizu, and T. Kubota, ''Image blur of edge-illuminated holograms,'' *Opt. Eng.* **37**, 241–246 (1998).
2. D. Psaltis, ''Coherent optical information systems,'' *Science* **298**, 1359–1363 (2002).
3. F. H. Mok, ''Angle-multiplexed storage of 5000 holograms in lithium niobate,'' *Opt. Lett.* **18**, 915–917 (1993).
4. D. Psaltis, M. Levene, A. Pu, G. Barbastathis, and K. Curtis, ''Holographic storage using shift multiplexing,'' *Opt. Lett.* **20**, 782–784 (1995).
5. R. S. Nesbitt, ''Edge-lit holography: Extending size and color,'' SM Thesis, Program in Media Arts and Sciences, Massachusetts Institute of Technology (1999).
6. D. G. Papazoglou, M. Loulakis, G. Siganakis, and N. A. Vainos, ''Holographic read-write projector of video images,'' *Opt. Express* **10**, 280–285 (2002).
7. W. C. Su, C. C. Sun, and N. Kukhtarev, ''Multiplexed edge-lit holograms,'' *Opt. Eng.* **42**, 1871–1872 (2003).
8. M. V. Moorthy, ''Numerical inversion of two-dimensional Laplace transforms-Fourier series representation,'' *Appl. Numer. Math.* **17**, 119–127 (1995).
9. J. Abate, G. L. Choudhury, and W. Whitt, ''Numerical inversion of multidimensional Laplace transforms by the Laguerre method,'' *Perform. Eval.* **31**, 229–243 (1997).
10. Q. Huang, P. P. Banerjee, M. R. Chatterjee, T. C. Poon, and H. J. Caulfield, ''Novel diffraction properties of a cross-beam generated volume hologram,'' *Gordon Conf. on Optical Signals Processing and Holography*, Plymouth NH (1993).
11. N. V. Kukhtarev, S. F. Lyuksyutov, P. Buchave, T. Kukhtareva, K. Sayano, and P. P. Banerjee, ''Self-enhancement of dynamic gratings in photogalvanic crystals,'' *Phys. Rev. A* **58**, 4051–4055 (1998).

Partha P. Banerjee is professor and chair of electrical and computer engineering at the University of Dayton. He received the BTech degree in electronics and telecommunication engineering from Indian Institute of Technology, Kharagpur, India in 1979. He received the MS and PhD degrees in electrical and computer engineering from the University of Iowa, in 1980 and 1983 respectively. He served as a faculty member at the University of Alabama in Huntsville from 1991 to 2000, and at Syracuse University from 1984 to 1991. His area of research interest is nonlinear optics and photorefractives. He is the recipient of the NSF Presidential Young Investigator Award in 1987. He is a fellow of the Optical Society of America and of SPIE, and is a senior member of IEEE. To date he has over 90 refereed journal publications and has authored four textbooks.

Monish R. Chatterjee is professor of electrical and computer engineering at the University of Dayton. He received the BTech degree in electronics and communications engineering from I.I.T., Kharagpur, India, in 1979. He received the MS and PhD degrees, both in electrical and computer engineering, from the University of Iowa, Iowa City, Iowa, in 1981 and 1985, respectively. He served as a faculty member at Binghamton University, the State University of New York from 1986 through 2002. As of Fall 2002, Dr. Chatterjee is with the ECE department at the University of Dayton. Dr. Chatterjee, who specializes in applied optics, has published more than 30 papers in archival journals. In addition, he has published more than 20 general-purpose articles on science in library reference books. Dr. Chatterjee received the State University of New York's Chancellor's Award for Excellence in Teaching in 2000. He is a senior member of IEEE, and a member of OSA, ASEE, and Sigma Xi.

Nickolai Kukhtarev is professor of physics at Alabama A&M University in Normal, AL. He received his MS in radiophysics and electronics from Kharkov University, Ukraine in 1966, his PhD from the Institute of Physics in Kiev, Ukraine in 1973, and his Habilitus in physical-mathematical sciences in 1983 from the Institute of Physics in Kiev for his work on dynamical holography. His research interests include nonlinear optics and photorefractives, self-organization, biological nonlinearities, and material characterization. He has published more than 150 refereed journal papers. He is a fellow of the Optical Society of America.

Tanya Kukhtareva is a research scientist in the department of physics and biology at Alabama A&M University. Her research interests include investigation of photorefractive crystals and polymers, single-beam holography, optical channeling by periodic structures, and optical methods for environmental applications. She has over 50 refereed journal publications and is a member of the Optical Society of America.